ADVANCED ELECTRONIC MATERIALS
www.advelectronicmat.de

Influence of DC Bias on the Hysteresis, Loss, and Nonlinearity of Epitaxial $PbZr_{0.55}Ti_{0.45}O_3$ Films

Philip Lucke, Muharrem Bayraktar, Niels Schukkink, Andrey E. Yakshin, Guus Rijnders, Fred Bijkerk, and Evert P. Houwman*

The hysteresis, loss, and nonlinearity of the strain and polarization response of an epitaxial $PbZr_{0.55}Ti_{0.45}O_3$ film are experimentally investigated for non-switching AC excitation fields at a DC bias of 20 kV cm^{-1} in the 70 Hz to 5 kHz range. The measured strain is hysteretic and linear, whereas the polarization is hysteretic and highly nonlinear with excitation amplitude. Furthermore, compared to the case with zero bias, the effective piezoelectric coefficient that is extracted from the strain response is almost not changed for the investigated field range. In contrast, the loss tangent and nonlinearity of the polarization response are strongly reduced. The observations can not be explained by the Rayleigh model and its extensions, but are very well explained by the recently proposed polarization rotation model through addition of a non-zero bias field term to the model. This model describes the film properties as the result of the nonlinear rotation of the polarization vector within the unit-cell in response to the applied field, which is accompanied with viscous domain interaction. These results demonstrate that the polarization rotation model can describe the film response in a broad range of excitation frequencies and amplitudes, which far the applicable range of the Rayleigh model.

1. Introduction

Hysteresis is a common challenge in the use of piezoelectric ceramics and thin films in applications such as sensors, actuators, ferroelectric memories, and energy harvesters.[1–8] Hysteresis can cause energy loss in energy harvesting devices or positioning inaccuracy in actuators.[9] Several studies have identified the viscous interaction of ferroelectric domains as the source of hysteresis and the associated dielectric/ferroelectric loss for sub-coercive field excitations.[10–14] However, this approach fails to explain the observed field amplitude dependence of the dielectric and piezoelectric loss tangents. For $PbZr_xTi_{1-x}O_3$ (PZT) ceramics and polycrystalline or chemical solution deposited (CSD) films, the amplitude and frequency dependent hysteresis behavior can be described by adapting the Rayleigh model, which has been used for the description of hysteresis in ferromagnets by considering the Barkhausen jumps.[15–18] In ferroelectrics the Rayleigh model considers the stochastic interaction of domain walls (DWs) with defects as jumps of the DWs from one energetic minimum to another analogous to Barkhausen jumps.[19,20] Because of its stochastic description, the Rayleigh model can not take into account the crystal symmetry of the material, which is expected to strongly influence the hysteresis, loss, and nonlinearity since the functional properties of the material are dependent on the crystal symmetry and, thus, on the growth orientation of an epitaxial film.[21] The Rayleigh model assigns a single parameter to describe the combined effect of nonlinearity and loss as the source of hysteresis. Even though the nonlinear response of some ceramics and CSD films can be described by the odd harmonics predicted by this model the even harmonics, which are also observed in some experiments can not be explained.[22,23] Other approaches such as time-dependent density functional theory can be used to explain the complex polarization effects, but they have to be extensively benchmarked with experimental data for practical use.[24,25]

In an earlier publication we have shown that for epitaxial $PbZr_{0.55}Ti_{0.45}O_3$ films with a monoclinic crystal symmetry, the hysteresis, loss, and nonlinearity of functional properties can be very well described by a model that considers the rotation of the polarization vector within the unit cell and that is accompanied by a viscous interaction of the domains.[26] Moreover, with this so-called polarization rotation model, it is possible to differentiate between the nonlinearity of the response that is caused by the nonlinear response of the angle of the polarization vector to the applied field and the loss due to viscous interaction of the domains. In addition, the polarization rotation model predicts all experimentally observed even and odd harmonics.

Applications usually work using a unipolar drive, which can be generated by using DC bias fields. As such, it is of

Dr. P. Lucke, Dr. M. Bayraktar, N. Schukkink, Dr. A. E. Yakshin, Prof. F. Bijkerk
Industrial Focus Group XUV Optics
MESA+ Institute of Nanotechnology
University of Twente
Enschede, P.O. Box 217, 7500 AE, The Netherlands
E-mail: m.bayraktar@utwente.nl
Prof. G. Rijnders, Dr. E. P. Houwman
Inorganic Material Science
MESA+ Institute of Nanotechnology
University of Twente
Enschede, P.O. Box 217, 7500 AE, The Netherlands
The ORCID identification number(s) for the author(s) of this article can be found under https://doi.org/10.1002/aelm.202100115.

DOI: 10.1002/aelm.202100115

importance to be able to describe the hysteresis and loss of the piezoelectric materials under this condition. Some papers using the Rayleigh model also report on the case of non-zero field bias. In these reports the applicable range of the Rayleigh model increases and the hysteresis decreases as bias increases.[27–30] However, the Rayleigh model does not allow to make quantitative predictions on the change of the Rayleigh parameters with applied bias. Here we experimentally show that for monoclinic, epitaxial $PbZr_{0.55}Ti_{0.45}O_3$ films, an extension of the polarization rotation model can quantitatively describe the hysteresis, loss, and nonlinearity in the strain and polarization also for non-zero bias fields.

2. Polarization Rotation Model with Applied Bias

The polarization rotation model considers the rotation of the polarization vector in the (110)-plane in a (001)-oriented rhombohedral or monoclinic thin films under the influence of an electric field excitation.[26] The polarization, measured across the film in a parallel plate capacitor configuration, is then given by

$$P = P_S \cos(\theta) \tag{1}$$

with P_S the length of the spontaneous polarization vector and θ the angle between the [001]-axis and the polarization vector. Using a grounded bottom electrode, a positive voltage on the top electrode corresponds to a downward-oriented electric field so that in a poled film the polarization angle is measured with respect to a top-to-bottom oriented film normal axis. In a fully relaxed unit cell at zero field, the polarization vector is in the body diagonal and θ equals $\theta_0 = 54.7°$. Our films are under compressive, in-plane stress, resulting in a rotation of the polarization vector (in zero field) toward the out-of plane direction and, thus, in a lower polarization angle that is defined as $\theta_{0,f}$[26] (the subscript f indicates that the sample is a clamped thin film). The associated polarization value is the remanent polarization $P_r = P_S \cos(\theta_{0,f})$ of the film. The application of a (positive) bias field in the [001]-direction leads to a further rotation of the angle θ toward the [001]-axis and is denoted by $\theta_{DC,f}$. The polarization is then $P_{DC} = P_S \cos(\theta_{DC,f})$. Under an additionally applied AC field in the [001]-direction, the angle of the polarization vector oscillates around $\theta_{DC,f}$, causing the oscillation of the polarization value around P_{DC}, and consequently stretching and contraction of the unit-cell, and thus an oscillating strain in the [001]-direction by the piezoelectric effect.

In the following, we first present the strain and polarization loops of the film in response to large electric field amplitudes far exceeding the coercive field. From these measurements the strain, polarization and polarization angle are described as a function of applied field in the non-switching range of the loop, that is in the field range commonly used in hysteresis measurements. From these descriptions the nonlinearity and loss tangent of the strain and polarization during hysteresis measurements are predicted based on an extension of the polarization rotation model by taking into account a non-zero bias field. Here we only consider polarization rotation and no polarization switching. Therefore, the magnitude of the AC and DC fields in the experiments are selected accordingly. Furthermore, we assume that for the used magnitudes of the AC and DC fields the extension of the polarization vector is negligible.[26,31,32]

2.1. Strain Response

Typical large signal strain–electric field (S-E) and polarization–electric field (P-E) loops are shown in **Figure 1**. For the

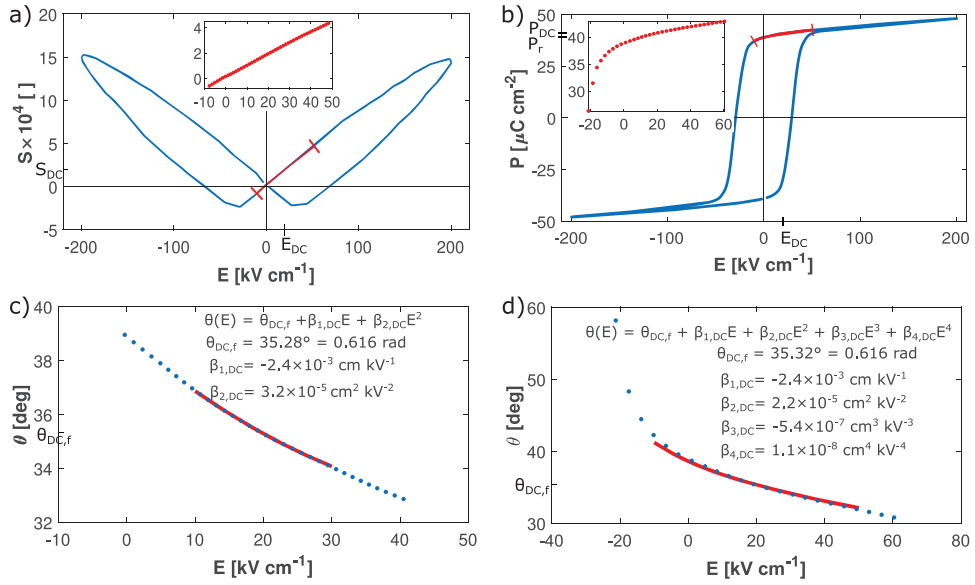

Figure 1. Global a) S-E and b) P-E loops. The red lines show the maximum trajectory of strain and polarization corresponding to AC cycling around the 20 kV cm^{-1} DC bias. The insets show the magnified view of these trajectories. Field dependence of the polarization angle θ calculated from the inset in (b) for AC field amplitudes of c) 10 kV cm^{-1} and d) 28 kV cm^{-1}. The red lines give the fit of the datapoints with (c) a second order polynomial in the 10 to 30 kV cm^{-1} field range and (d) a fourth order polynomial in the –8 to 48 kV cm^{-1} field range. All measurements are at 3 kHz.

hysteresis measurements we consider a downward polarized sample driven by an AC field excitation on top of a zero or positive field bias, such that the polarization (strain) oscillates along the falling branch of the large signal P-E (S-E) loop. A positive DC bias of 20 kV cm^{-1} during the hysteresis measurements causes the central point of the AC field oscillations (with amplitudes in the range of 2.5–28 kV cm^{-1}) to shift along the field axis. The strain and polarization values shift accordingly on the global S-E and P-E loops as shown with red lines in Figure 1a,b. The measured strain around the bias field is in good approximation (R^2 = 0.9994) linear with the applied field, as shown in the inset. Therefore, we can describe the DC strain by the linear relation $S_{DC} = d_{33,f}E_{DC}$ where $d_{33,f}$ and E_{DC} are respectively the effective piezoelectric coefficient in the out-of-plane direction of the clamped thin film and the applied DC bias field. One can then also describe the AC strain response by a linear relation that is in-phase (ip) with the applied AC field $E(t)$, thus, $S_{ip}(t) = d_{33,f}E(t)$ for oscillating fields that do not extend beyond the sub-coercive field similar as was done for the zero bias case. The validity of the linear dependence can be derived from the Landau–Devonshire model to a good approximation.[26] The observation of elliptic strain hysteresis loops in our experiments suggests that the piezoelectric loss is dominated by a viscous loss mechanism.[26] The viscous loss can be introduced as an out-of-phase (oop) component in the strain response which is proportional to the time derivative of the in-phase response as $S_{oop}(t) = \gamma_S \dot{S}_{ip}(t)$, where γ_S is a viscosity coefficient. The total strain is then the sum of S_{DC}, S_{ip}, and S_{oop}

$$S(E) = d_{33,f}E_{DC} + d_{33,f}E + \gamma_S d_{33,f}\dot{E} \tag{2}$$

One arrives at a simple expression for the strain response to a small amplitude sinusoidal field, $E(t) = E_0 \sin(\omega t)$, similar to that for the zero bias case apart from the S_{DC} offset.

$$S(t) = d_{33,f}E_{DC} + d_{33,f}E_0 \sin(\omega t) + \gamma_d \omega E_0 \cos(\omega t) \tag{3}$$

Here we defined $\gamma_d = \gamma_S d_{33,f}$. It is noted that in the following experiments use is made of a double beam laser interferometer (DBLI), which allows only the determination of strain changes, hence, the value of S_{DC} can not be determined. However, this does not change the validity of the model as the DC component of the strain only works as an offset and does not influence the scaling of loss or hysteresis. As a consequence of the assumed viscous nature of the loss process the unit cell deformation is lagging in time in response to varying fields, thus, one expects that $\gamma_d < 0$. We do not exclude the presence of any implicit frequency dependencies of the parameters $d_{33,f}$ and γ_d, which could stem from frequency dependent viscous interactions. However, the nature of such interactions is poorly understood and described in literature. Instead, we will extract the frequency dependence of these parameters from the hysteresis measurements at different frequencies.

The strain loss, or loss tangent, is simply given by the ratio of the viscous to non-viscous components of the strain:

$$\tan\delta_S = |\gamma_d \omega / d_{33,f}| = |\gamma_S \omega| \tag{4}$$

2.2. Polarization Response

A typical global P-E loop is shown in Figure 1 b. For the hysteresis measurements we consider only the decreasing field branch, because the film is poled downward before each measurement. The application of a positive DC field bias of +20 kV cm^{-1} leads to a shift of the center point of the AC polarization response to the value $P = P_{DC}$. The hysteresis measurements have been performed with AC field amplitudes from 2.5 to 28 kV cm^{-1}. For the analysis of the nonlinearity we used two AC field amplitudes, 10 and 28 kV cm^{-1}. The lower amplitude is chosen to be the same as in Lucke et.al.[26] to be able to compare the zero bias case to non-zero bias case. The large amplitude was chosen because it is the largest amplitude that can be used without observable effects of polarization switching on the hysteresis. This amplitude results in an oscillation of the electric field from –8 to 48 kV cm^{-1} that enables to explore the validity of the polarization rotation model in a field range that is far exceeding the Rayleigh range. The red line in Figure 1b shows the maximum range of field and polarization change for the second AC amplitude.

The change of the polarization angle θ around $\theta_{DC,f}$, which is in-phase with the driving field, is described by $\theta_{ip} = \Delta\theta(E(t))$. The out-of-phase part is described as $\theta_{oop} = \gamma_P \Delta\dot{\theta}$, assuming a linear viscous interaction with viscosity coefficient γ_P to be present. The change of the polarization angle is then given by the summation of the three contributions.

$$\theta(E) = \theta_{DC,f} + \Delta\theta(E) + \gamma_P \Delta\dot{\theta}(E) \tag{5}$$

The change of the polarization angle that is in-phase with the applied field can be described with a polynomial that has the general form:

$$\Delta\theta(E) = \beta_{1,DC}E + \beta_{2,DC}E^2 + \beta_{3,DC}E^3 \ldots = \sum_{i=1}^{p}\beta_{i,DC}E^i \tag{6}$$

where p is the order of the polynomial. The value of p in the first place depends on the AC amplitude E_0 but also on the strain state of the film and consequently on the substrate, the deposition temperature, and the film composition since these change the curvature of the P-E loop. Because the polarization angle decreases with increasing field the odd β coefficients should be negative. The even β coefficients give rise to a possible asymmetry in the field sensitivity of $\Delta\theta(E)$ around $\theta_{DC,f}$. Furthermore, the viscosity parameter γ_P is expected to be negative as the out-of-phase response should lag behind the electric field.

Figure 1c,d gives the angle $\theta(E)$ that is calculated from the global P-E loop using Equation (1). For both AC amplitudes the curves are fitted with a polynomial of order two (R^2 = 0.9999) and four (R^2 = 0.9997), respectively. These are the lowest order polynomials that can accurately describe the nonlinearity of the measured $\theta(E)$. The fit values of the polynomial coefficients that will be used further on in this study are given in Figure 1c,d. It is seen that the expectations with respect to the signs of the coefficients match with the signs of the fitted values. Furthermore, the increase in the AC field amplitude just leads to an increase of the order of the polynomial p because the covered

part of the $\theta(E)$-curve becomes increasingly curved, but the β_p parameters remain of the same order of magnitude for different AC amplitudes.

A comparison of the fitted polynomials for AC amplitude of 10 kV cm^{-1}, with and without DC bias, shows that the order of the polynomial decreases from 4 to 2 for the non-zero bias case.[26] Moreover, with zero bias the values of the β-coefficients ($\beta_1 = -3.9 \times 10^{-3}$ cm kV^{-1} and $\beta_2 = 1.1 \times 10^{-4}$ cm^2 kV^{-2} [26]) are significantly larger than the corresponding $\beta_{i,\mathrm{DC}}$-coefficients in Figure 1c because of the increased average slope and asymmetry of the P-E loop for zero bias.

Inserting Equations (5) and (6) into Equation (1) and using some trigonometric identities the dependence of the polarization on the angular change $\theta(E)$ with applied DC bias can be written as:

$$\begin{aligned} P\left(\theta(E)\right) &= P_{\mathrm{S}} \cos\left(\theta_{\mathrm{DC},f} + \Delta\theta + \gamma_P \Delta\dot{\theta}\right) \\ &= P_{\mathrm{DC}}\left[\cos\left(\Delta\theta + \gamma_P \Delta\dot{\theta}\right) - \tan\left(\theta_{\mathrm{DC},f}\right)\sin\left(\Delta\theta + \gamma_P \Delta\dot{\theta}\right)\right] \end{aligned} \tag{7}$$

Here $P_{\mathrm{DC}} = P_{\mathrm{S}} \cos(\theta_{\mathrm{DC},f})$. From Figure 1c,d it can be seen that $\Delta\theta(E)$ is of the order of a few degrees allowing the use of lowest order Taylor expansions of the sin and cos functions. This approximation results in a nonlinear, analytically tractable, polynomial expression for the time-dependent polarization response which can be written concisely as a sum of sine and cosine functions that depends on the order p of the $\Delta\theta(E)$ polynomial:

$$P(t) = P_{\mathrm{DC}}\left[c_0 + \sum_{n=1}^{2p} c_{n,s} E_0^n \sin(n\omega t) + c_{n,c} E_0^n \cos(n\omega t)\right] \tag{8}$$

The coefficients of the harmonics c_0, $c_{n,s}$ and $c_{n,c}$ are functions of the polynomial parameters $\beta_{i,\mathrm{DC}}$, viscosity coefficient γ_P, the AC field frequency ω and the AC field amplitude E_0. In Section S1, Supporting Information, explicit forms of these functions are given. Note that all coefficients are even functions of E_0 and that the amplitude of the harmonics rapidly decreases with increasing harmonic number n. The $\sin(n\omega t)$ terms give rise to peaks in the frequency domain at all frequencies $n\omega$, with $n = 1$ being the fundamental harmonic and $n > 1$ being the corresponding higher harmonics. Thus, the model predicts that in the polarization signal all harmonics are present up to fourth and eight order for E_0 = 10 and 28 kV cm^{-1} respectively. Furthermore, hysteresis is expected to be present in all harmonics, since for every harmonic there is a non-zero cosine term in the expansion.

It is found from calculation using the determined coefficients that $c_0 \approx 1$ for all used amplitudes and frequencies. Consequently, the first and higher order hysteresis loops are all centered around the same bias point P_{DC}. The amplitude of the nth polarization harmonic in the case of applied bias can be calculated by:

$$\left|P_{n,\mathrm{DC}}(E_0)\right| = P_{\mathrm{DC}}\left(E_0^n \sqrt{c_{n,s}^2 + c_{n,c}^2}\right) \tag{9}$$

One can now predict the scaling of $|P_{n,\mathrm{DC}}(E_0)|$ with the AC field amplitude from the E_0 dependence of the c-coefficients. For $E_0 <= 10$ kV cm^{-1} the harmonic amplitudes are predicted to scale as:

$$\begin{aligned} \left|P_{1,\mathrm{DC}}(E_0)\right| &= P_{\mathrm{DC}}\left(k_{1,1}E_0 + k_{1,3}E_0^3\right) \\ \left|P_{2,\mathrm{DC}}(E_0)\right| &= P_{\mathrm{DC}}\left(k_{2,2}E_0^2 + k_{2,4}E_0^4\right) \\ \left|P_{3,\mathrm{DC}}(E_0)\right| &= P_{\mathrm{DC}}\left(k_{3,3}E_0^3\right) \\ \left|P_{4,\mathrm{DC}}(E_0)\right| &= P_{\mathrm{DC}}\left(k_{4,4}E_0^4\right) \end{aligned} \tag{10}$$

The $k_{n,m}$ coefficients are new functions of the β-coefficients and ω, where n is again the order of the harmonic and m is the power of the corresponding field amplitude term. The predicted scaling of the polarization amplitude for $E_0 <= 10$ kV cm^{-1} with E_{DC} = 20 kV cm^{-1} bias is less nonlinear than for the same AC amplitude with zero bias as the model predicts additional 5th and 6th order harmonics for the latter case and only up to 4th order for the DC bias case.

For $E_0 <= 28$ kV cm^{-1} the harmonic amplitudes are predicted to scale as:

$$\begin{aligned} \left|P_{1,\mathrm{DC}}(E_0)\right| &= P_{\mathrm{DC}}\left(k_{1,1}E_0 + k_{1,3}E_0^3 + k_{1,5}E_0^5\right) \\ \left|P_{2,\mathrm{DC}}(E_0)\right| &= P_{\mathrm{DC}}\left(k_{2,2}E_0^2 + k_{2,4}E_0^4 + k_{2,6}E_0^6\right) \\ \left|P_{3,\mathrm{DC}}(E_0)\right| &= P_{\mathrm{DC}}\left(k_{3,3}E_0^3 + \left(k_{3,5}E_0^5\right)\right. \\ \left|P_{4,\mathrm{DC}}(E_0)\right| &= P_{\mathrm{DC}}\left(k_{4,4}E_0^4 + k_{4,6}E_0^6\right) \\ \left|P_{5,\mathrm{DC}}(E_0)\right| &= P_{\mathrm{DC}}\left(k_{5,5}E_0^5\right) \\ \left|P_{6,\mathrm{DC}}(E_0)\right| &= P_{\mathrm{DC}}\left(k_{6,6}E_0^6\right) \\ \left|P_{7,\mathrm{DC}}(E_0)\right| &= P_{\mathrm{DC}}\left(k_{7,7}E_0^7\right) \\ \left|P_{8,\mathrm{DC}}(E_0)\right| &= P_{\mathrm{DC}}\left(k_{8,8}E_0^8\right) \end{aligned} \tag{11}$$

There is a clear increasing nonlinear dependence of the polarization response on E_0 because of the presence of higher order polynomial terms and an increase of the number of harmonics. Overall, the amplitude of the harmonics scale either with even or odd powers of the field amplitude depending on the parity of the order of the harmonic. This relation was also found for the zero bias case.[26]

The energy loss per polarization hysteresis cycle is proportional to the area enclosed by the hysteresis loop in the field domain, $\int_{\mathrm{cycle}} P(E)\mathrm{d}E$. It appears that only the fundamental harmonic has a non-zero area as the areas of all higher harmonics are described by integrals of the product of an even and an odd function and is as such zero (see Section S2, Supporting Information for further details). The polarization loss tangent $\tan\delta_{\mathrm{P}}$ can therefore be calculated simply as the ratio of the coefficients of the viscous and non-viscous part of the fundamental harmonic:

$$\tan\delta_{\mathrm{P}} = \left|\frac{c_{1,c}}{c_{1,s}}\right| \approx \left|\gamma_P \omega\right| \tag{12}$$

It is easy to show that the last approximation step holds by substituting the numerical values in the expressions of $c_{1,c}$ and

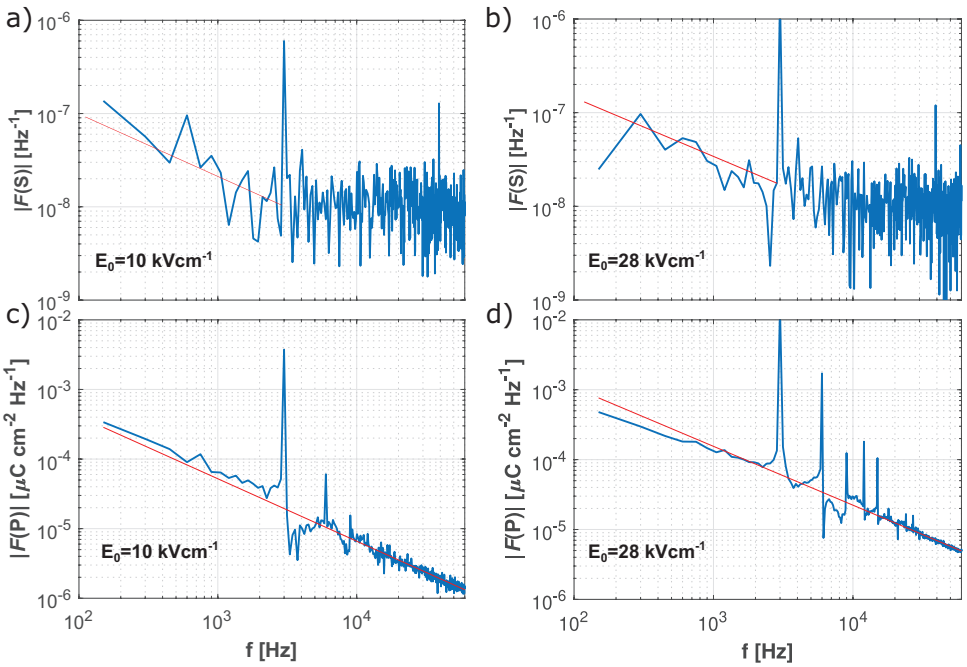

Figure 2. Fourier transform of a,b) the measured strain and c,d) the polarization signal for a sinusoidal signal of 20 cycles at 3 kHz. Respectively, left and right columns show the signal for AC field amplitudes of 10 and 28 kV cm^{-1}. The red line indicates the fitted 1/*f* noise baseline.

$c_{1,s}$. This is the same expression as for the strain loss tangent and for the zero bias case.[26]

3. Results and Discussion

Figure 2 shows the Fourier Transform of the measured strain and polarization signal in response to a sinusoidal driving field at 3 kHz. The left and right columns show the signals for E_0 = 10 and 28 kV cm^{-1} respectively for a bias field of E_{DC} = 20 kV cm^{-1}. The raw strain data in Figure 2a,b show only a single peak at the fundamental frequency of 3 kHz. No higher harmonics can be identified. (Some high amplitude noise peaks appear at higher frequencies, but because of their very narrow peak width we attribute these to numerical artifacts of the fast Fourier transform algorithm.) Below 2 kHz one can clearly observe a frequency dependent noise that is inversely proportional to the frequency. The polarization signal, Figure 2c,d, shows several higher harmonics superimposed on the frequency dependent background noise. For small and large E_0 respectively all harmonics up to 3rd and 9th order are observed in agreement with the predictions of the the polarization rotation model in Equations (10) and (11). Not observing the predicted 4th order harmonic for the low E_0 case can be explained by the rapidly declining amplitude of the harmonics, such that the 4th harmonic is hidden in the noise, see Section S1.1, Table S1, and Figure S1, Supporting Information. The observation of a 9th order harmonic for the high E_0 case when the model predicts only harmonics up to 8th order is related to the choice of the lowest order polynomial. A higher order polynomial would lead to higher orders but would also make the equations too complicated to follow. The observed frequency dependent noise was fitted with a power law dependence $P_{noise}(f) = af^b$ in the polarization data where the frequency dependent noise is more apparent. The exponent was obtained as $b = -0.89 \pm 0.03$ by taking into account all the polarization measurements indicating the 1/*f* character of the noise. The obtained 1/*f* baseline is also overlaid to the strain signal below the fundamental frequency. The 1/*f* baseline closely matches the observed frequency dependent baseline for both the polarization and the strain in Figure 2.

3.1. Strain Hysteresis Measurements

The low frequency noise in the strain data hinders an accurate fit of the model to the raw measurement data. For this reason the strain signal was band-pass filtered around the fundamental harmonic and then averaged over the measured 20 cycles.[26] In **Figure 3** the strain signals (markers) and the fits using Equation (3) (lines) are shown for four amplitudes. For clarity only every fifth data point is shown. The standard deviation of the filtered and averaged data points with respect to the fit is smaller than the size of the markers. The strain hysteresis loops in Figure 3b are elliptical in contrast to the lenticular shapes expected from the Rayleigh model. The data and fits for the other frequencies are shown in the Section S3, Supporting Information. For all amplitudes and frequencies the linear, viscous strain model accurately fits the data.

The extracted model parameters $d_{33,f}(E_0 f)$ and $\gamma_d(E_0 f)$ at 3 kHz frequency are plotted as a function of the field amplitude E_0 in **Figure 4**a,b. The statistical uncertainty of the fitted parameters is smaller than the size of the markers. One observes no obvious field dependence of $d_{33,f}$ and γ_d. Both model parameters fluctuate around an average value, that is the average of the model parameters at different E_0 that can be represented

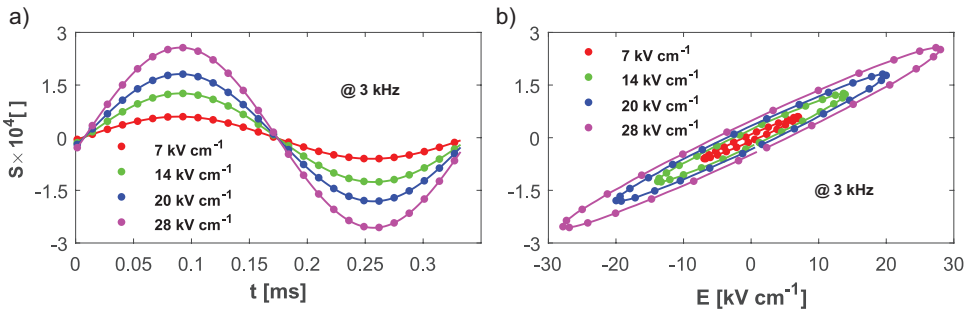

Figure 3. Filtered and averaged strain signal as function of a) time and b) applied cyclic field, $E(t)$. Datapoints show the measurement and the lines are obtained from fitting with Equation (3).

by $\langle d_{33,f} \rangle_{E_0}$ (3 kHz) and $\langle \gamma_d \rangle_{E_0}$ (3 kHz) and indicated by the solid lines in the figure. The shaded areas indicate the $\pm 2\sigma$ confidence intervals of the averages. The average values are $\langle d_{33,f} \rangle_{E_0}$ (3 kHz) = 88 pm V^{-1} and $\langle \gamma_d \rangle_{E_0}$ (3 kHz) = -9×10^{-11} cm kV^{-1} Hz^{-1} rad^{-1}.

Figure 4c shows the dependence of the loss tangent on the excitation field amplitude. The datapoints are calculated from the area of the hysteresis loop measured for that E_0 value. The lines correspond to the loss tangent calculated using Equation (4) with the field averaged values $\langle d_{33,f} \rangle_{E_0}$ (3 kHz) and $\langle \gamma_d \rangle_{E_0}$ (3 kHz). The confidence intervals (shaded areas) are calculated using the error propagation of the confidence interval of these parameters. The measured loss tangent data shows much less spread than the $\pm 2\sigma$ confidence interval except for those at the lowest E_0 values. We conclude that within the measurement accuracy the loss tangent is independent of the excitation amplitude as is expected on the basis of the model if $d_{33,f}$ and γ_d are independent of the field amplitude. Experimentally we also find that $d_{33,f}$, γ_d, and tan δ_S, within the investigated amplitude range, are independent of the AC field amplitude. This also implies that the global S-E loop in the –8 to 48 kV cm^{-1} range is linear, as was already observed in Figure 1a. The data for the zero bias case is plotted in blue in Figure 4 for comparison with the 20 kV cm^{-1} bias case. We observe that the application of a bias field has no significant effect on the values of the strain parameters. It is seen that the average $\langle d_{33,f} \rangle_{E_0}$ (3 kHz) decreases from 96 pm V^{-1} for the zero bias case to 88 pm V^{-1} for the bias case which means that the average slope in the range –10 to 10 kV cm^{-1} is slightly larger than in the range –8 to 48 kV cm^{-1}. We do not attribute any significance to the small difference in average γ_d and tan δ_S values since the differences are within the confidence intervals.

In **Figure 5**a,b the averaged values $\langle d_{33,f} \rangle_{E_0}$ and $\langle \gamma_d \rangle_{E_0}$ are shown as a function of the excitation frequency. The error bars denote the standard deviation of these parameters over the investigated field range for that frequency. Orange and blue colors are used for the bias and zero bias case respectively. It is seen that $\langle d_{33,f} \rangle_{E_0}$ and $\langle \gamma_d \rangle_{E_0}$ are also independent of frequency. The field and frequency averaged values, $\langle d_{33,f} \rangle_{E_0,\omega}$ and $\langle \gamma_d \rangle_{E_0,\omega}$ and the corresponding confidence intervals are denoted by the horizontal lines and the shaded areas respectively. The field and frequency averaged value of the piezoelectric

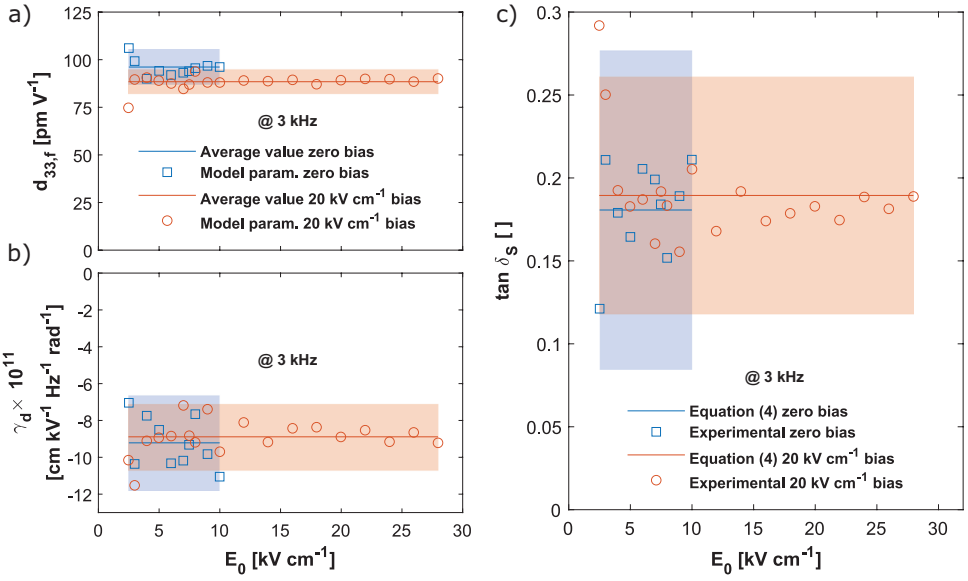

Figure 4. Field amplitude dependence of the parameters a) $d_{33,f}$ and b) γ_d for zero bias (blue) and 20 kV cm^{-1} bias (orange). The lines denote the average value $\langle d_{33,f} \rangle_{E_0}$ and $\langle \gamma_d \rangle_{E_0}$ and the shaded areas indicate the $\pm 2\sigma$ confidence intervals. c) tan δ_S calculated from the area of the hysteresis loops. The lines and confidence intervals are calculated with Equation (4) using the data in (a) and (b).

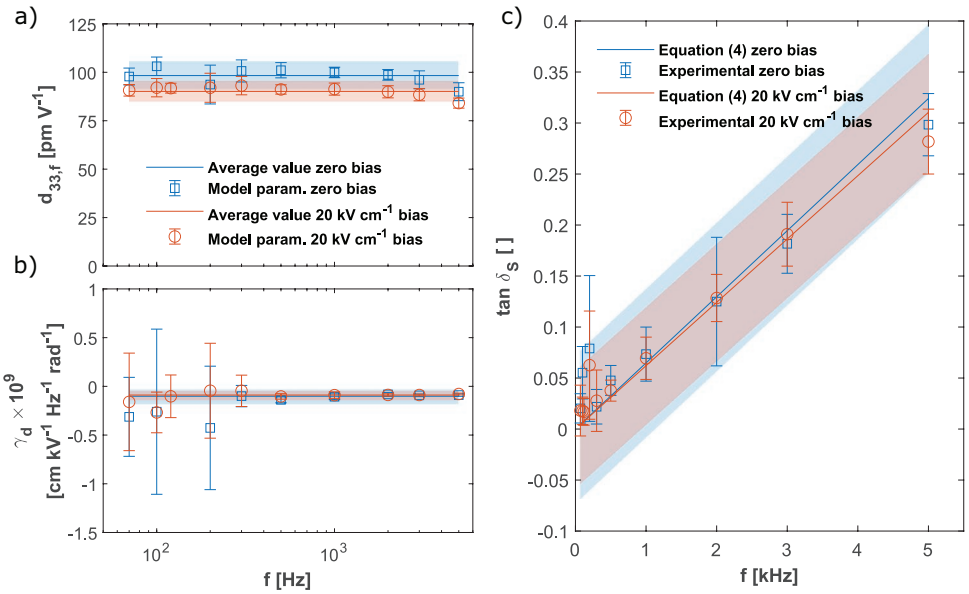

Figure 5. a) Average piezoelectric coefficient $\langle d_{33,f}\rangle_{E_0}$ and b) viscosity parameter $\langle \gamma_d \rangle_{E_0}$ for zero bias (blue) and 20 kV cm^{-1} bias (orange). The error bars denote the standard deviation of the field averaged values. The lines and shaded areas indicate the averages ($\langle d_{33,f}\rangle_{E_0,\omega}$ and $\langle \gamma_{d,}\rangle_{E_0,\omega}$) and their $\pm 2\sigma$ confidence intervals, respectively. c) Loss tangent data points are calculated from the area of the hysteresis loops. The lines and shaded confidence intervals are calculated from the average values in (a) and (b) using Equation (4).

coefficient is $\langle d_{33,f}\rangle_{E_0,\omega} = 90$ pm V^{-1}. For $\langle \gamma_d \rangle_{E_0}$ the low frequency data show larger error bars which is attributed to the large 1/*f*-noise at these frequencies. The field and frequency averaged value is $\langle \gamma_d \rangle_{E_0,\omega} = -10 \times 10^{-11}$ cm kV^{-1} Hz^{-1} rad^{-1}, so that the viscosity coefficient for strain is obtained as $\langle \gamma_S \rangle_{E_0,\omega} = -1.1 \times 10^{-5}$ Hz^{-1} rad^{-1}.

In **Figure 5**c the field averaged loss tangent values are shown as a function of the frequency. Again the loss tangent is calculated from the area of the hysteresis loops and the error bars denote the standard deviation of the data for different E_0-values. The lines are calculated with Equation (4) using the field and frequency averaged values $\langle d_{33,f}\rangle_{E_0,\omega}$ and $\langle \gamma_d \rangle_{E_0,\omega}$. The $\pm 2\sigma$ confidence intervals are calculated from the error propagation of the $\pm 2\sigma$ confidence intervals in Figure 5a,b. It is observed that the experimental loss tangent scales linearly with frequency as expected from Equation (4) which supports the assumption of a viscous loss mechanism for the strain.

Our results clearly show that the model parameters $d_{33,f}$, γ_d and, thus, γ_S are independent of the excitation field amplitude and frequency. Furthermore, we observe that the application of a bias field does not lead to a significant change of the values of these parameters and the loss tangent. As already remarked previously, the Rayleigh model cannot explain the observed frequency and amplitude dependencies of the loss tangent while these follow naturally from our model, assuming a frequency and amplitude independent viscosity constant γ_S.

3.2. Polarization Hysteresis Measurements

The amplitudes of the first and higher harmonics (up to 5th harmonic) of the polarization signal are plotted as function of the field amplitude E_0 in **Figure 6**. For harmonics with $n > 5$ the amplitude is below the 1/*f*-noise baseline, except for the largest value of E_0. The lines are fits for the zero bias (blue) and 20 kV cm^{-1} bias case (orange), using Equation (11). The only constraint imposed on the fits is that the $k_{n,m}$ coefficients are positive, as is expected from the model. Clearly, the fitted polynomials describe accurately the experimentally observed field dependencies, demonstrating the applicability of the model. Figure 6 shows that the P_n for all harmonics at the zero bias case increases rapidly with increasing field amplitude compared to the non-zero bias case.

It is noted that it is not possible to describe the amplitudes of the harmonics in terms of the determined β-coefficients because the harmonic peaks in the measured Fourier spectra show considerable frequency spreading implying significant energy transfer from the harmonic frequency to the neighboring frequencies. This mechanism is not taken into account in the model and causes a discrepancy between the theoretical and experimental values of the $c_{n,s/c}$ coefficients and, thus, of the $k_{n,m}$ coefficients. Nevertheless, as was already concluded for the case of zero bias the Rayleigh model cannot explain the presence of all even and odd harmonics of the polarization hysteresis. Furthermore, the third and higher order odd harmonics are clearly not scaling with E_0^2 as predicted by the Rayleigh model, but with higher order E_0^m dependencies.

The loss behavior as described by the polarization rotation model is determined by the fundamental harmonic only, Equation (12). In good approximation the polarization response can be described by the fundamental harmonic only because the $c_{n,s/c}$ coefficients for the higher harmonics ($n > 1$) rapidly decrease in value as compared to the fundamental harmonic ($n = 1$), thus,

$$P \approx P_{DC}[c_{1,s} E_0 \sin(\omega t) + c_{1,c} E_0 \cos(\omega t)] \quad (13)$$

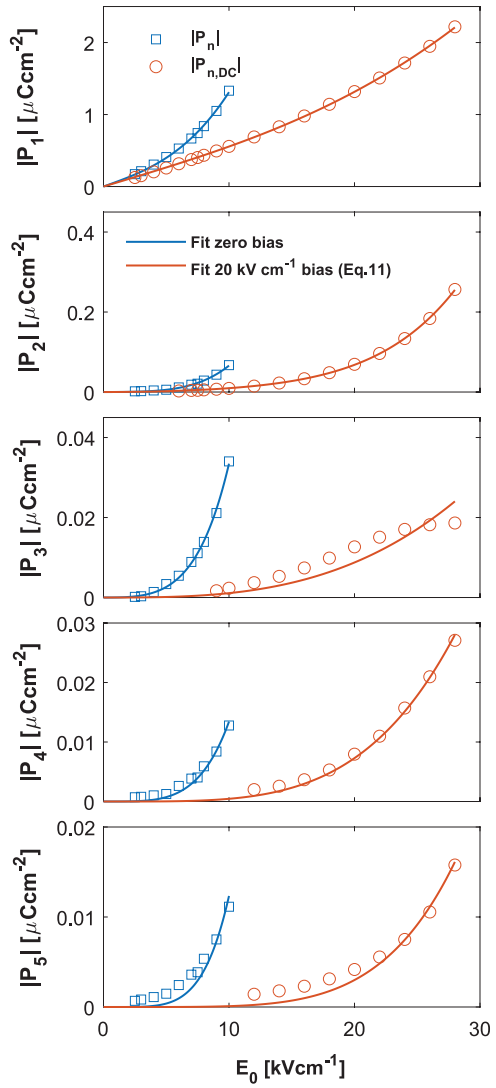

Figure 6. Scaling of the amplitude of the polarization harmonics with the field amplitude E_0. The data points are obtained from Fourier spectra of the polarization signal, such as shown in Figure 2 and the lines are fits to Equation (11). The orange and blue colors represent the bias and zero bias case, respectively.

Therefore, one can fit the measured hysteresis loops with the fundamental harmonic only to extract simply the values for $c_{1,s}$ and $c_{1,c}$ from which $\tan\delta_P$ can be calculated straightforwardly. The polarization hysteresis loops are obtained by high-pass filtering the signal and then averaging over the 20 measured cycles. The filtered data and the fits for a frequency of 3 kHz are shown in **Figure 7**a,b and for other frequencies in Section S4, Supporting Information. The good fits of the polarization against time or field demonstrate that the contributions from the higher harmonics are not observable except for the high applied field values, thus, that Equation (13) gives an accurate approximation of the polarization hysteresis signal. Only for $E_0 \geq 20$ kV cm^{-1} one observes deviations from the fit with the fundamental harmonic. In these cases the magnitude of the second harmonic in the Fourier spectrum becomes comparable to that of the fundamental frequency.

The polarization loss tangent calculated with Equation (12) is shown in **Figure 8**a,b as a function of field amplitude and frequency respectively. The loss tangent increases strongly with the increasing field amplitude. The polarization rotation model does not explicitly predict the observed field dependence but only a frequency dependence $|\omega\gamma_P|$ for a constant γ_P. There is a very weak explicit field dependence through the non-approximated version of the ratio $|c_{1,c}/c_{1,s}|$ which in fact would produce a opposite trend, that is a slight decrease of the loss tangent with increasing E_0. We neglect here this weak field dependence of the viscous loss term. Formally, one can absorb the field dependence of the loss tangent in a field dependence of the viscosity parameter as in Lucke et.al.[26] However, it is not possible to include the non-zero offset in the frequency plots in this way. Moreover, since we did not find a field dependence for the strain loss tangent, we think that the field dependence is not part of the viscous loss but can be attributed to an additional loss mechanism which is only present in the polarization hysteresis and described by $\tan\delta_E = cE_0^2$. Although a linear description would fit equally well the bias case, we assume that the loss mechanism is the same as for the zero bias case, where a quadratic fit was required, therefore, we use the same functional dependence on the field.[26] Comparing the loss tangent for the bias and zero bias cases in Figure 8a shows that the loss tangent is drastically reduced when a bias field is applied. For example, at $E_0 = 10$ kV cm^{-1} the loss tangent in the case of bias is reduced by about a factor 3 which we attribute to the reduction of the prefactor c of the field dependent term which is, thus, a function of the bias point $c(E_{DC})$.

The frequency dependence of the loss tangent at different field amplitudes is shown in Figure 8b. The loss tangent increases linearly with frequency for frequencies above about 500 Hz, while below this frequency the loss tangent increases slightly with decreasing frequency, suggesting a loss mechanism that may be related to 1/*f*-noise. We will not consider the latter any further here. The linear dependence above 500 Hz is typical for a viscous loss process and is predicted by the polarization rotation model in Equation (12). Above, we already showed that the amplitude dependence leads to a loss tangent contribution, $\tan\delta_E = cE_0^2$ while we also need to add a constant loss tangent, $\tan\delta_0$, to describe the offset of the viscous loss. For frequencies above about 500 Hz the total polarization loss tangent can now approximately be described with:

$$\tan\delta_P(E_0,\omega) \approx |\gamma_P\omega| + cE_0^2 + \tan\delta_0 \quad (14)$$

To extract the model parameters of Equation (14), we have fitted the frequency dependence from 500 Hz to 5 kHz with a linear function, $\tan\delta_P(E_0,\omega) = \tan\delta_0^*(E_0) + |\gamma_P\omega|$, where $\tan\delta_0^*$ is a free fitting parameter depending on the field amplitude. A single γ_P value is obtained from simultaneous fitting of all curves by least-square fitting. This procedure is allowed since the viscous contribution is assumed to be independent of E_0. The resulting linear fits are shown in Figure 8b by the lines and well describe the measured data. To extract $\tan\delta_0$ and c the resulting $\tan\delta_0^*(E_0)$ values are fitted with $\tan\delta_0^*(E_0) = cE_0^2 + \tan\delta_0$ as shown in Section S5, Supporting Information. For a bias of 20 kV cm^{-1} the fit parameters are $\gamma_P = -3.27 \times 10^{-6}$ rad^{-1} Hz^{-1}, $c = 1.46 \times 10^{-4}$ kV^{-2} cm^2, and

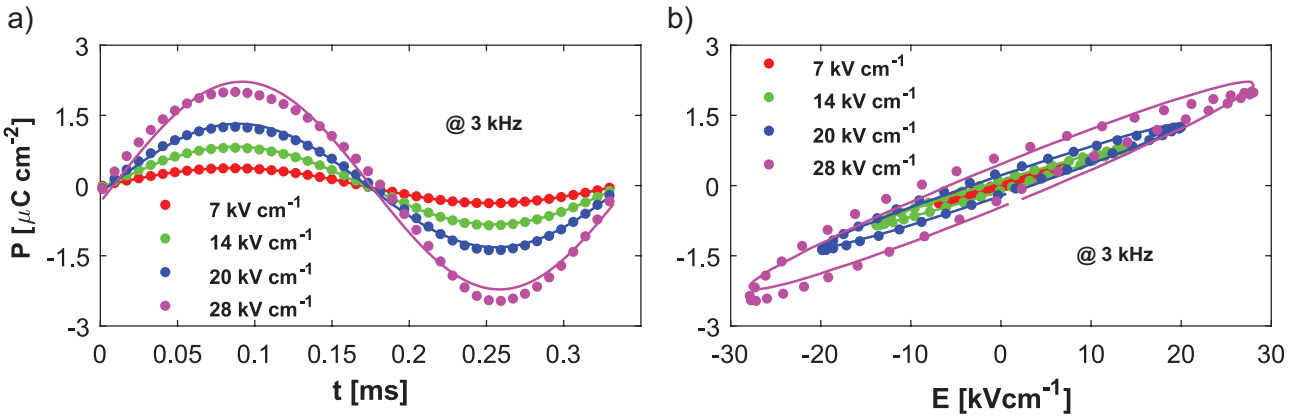

Figure 7. Filtered and averaged polarization hysteresis signal as function of a) time and b) applied AC electric field. The markers represent the measured data, which include all higher harmonics, and the solid lines are obtained by fitting to Equation (13).

$\tan\delta_0 = 4.34 \times 10^{-2}$. The same fitting procedure is repeated for the zero bias case, resulting in the fit parameters $\gamma_P = -2.26 \times 10^{-6}$ rad^{-1} Hz^{-1}, $c = 2.59 \times 10^{-3}$ kV^{-2} cm^2, and $\tan\delta_0 = 6.53 \times 10^{-2}$. The fits are shown in Section S5, Supporting Information. We observe that the application of a bias slightly changes γ_P, and $\tan\delta_0$ whereas the c-parameter is a factor 18 larger for the zero bias case. We attribute these differences to the much stronger curvature of the polarization loop at zero bias and, therefore, stronger dependence of the polarization angle on the AC-field amplitude. Using these fit parameters and Equation (14) the lines in Figure 8a are generated and we observe that our model describes the measured loss tangent very well for the bias and zero bias case. These results strongly suggest that there are multiple loss mechanisms at play simultaneously in the polarization hysteresis: a viscous loss arising from the proposed polarization rotation model that accounts for the strong frequency dependence, a yet unexplained field dependent loss and an unexplained constant loss contribution. We note that the different loss mechanisms all appear to give rise to an elliptically shaped hysteresis loop, thus, that they can be described by a relation like Equation (13), that is with a 90° out-of- phase response term and not by a Rayleigh-like description, which would give rise to more lenticular-shaped hysteresis loops.

Above, we have applied the polarization rotation model, introduced in Lucke et al., to describe the strain and polarization hysteresis in the same sample as discussed there, for the case of non-zero bias, by adding a DC-bias field term.[26] Furthermore, we have used the model to a much wider applied field range, that is in the range from −8 to 48 kV cm^{-1}. It is found that, although, the strain response is hysteretic the amplitude of the strain response has a linear relation with the applied field and no higher strain harmonics are observed. The strain response can, therefore, be described by a linear response model including a viscous loss proportional to the velocity of the strain change, $\Delta\dot{S}$. Moreover, it is found that the parameters appearing in the hysteresis model, that is the effective piezoelectric coefficient $d_{33,f}$ and the strain loss parameter γ_S do not depend on excitation frequency and amplitude in the investigated range. Consequently, the loss tangent of the strain hysteresis process is simply given by the product of a constant γ_S and the angular frequency, $\tan\delta_S = |\omega\gamma_S|$. Contrary to the strain, the response of the polarization angle θ to the applied field is highly nonlinear. This causes many higher order harmonics in the polarization hysteresis signal. The model describes the polarization hysteresis with a viscous loss proportional to the velocity by which the polarization angle rotates $\Delta\dot{\theta}$, with a viscosity coefficient γ_P. However, experimentally an additional term quadratic in

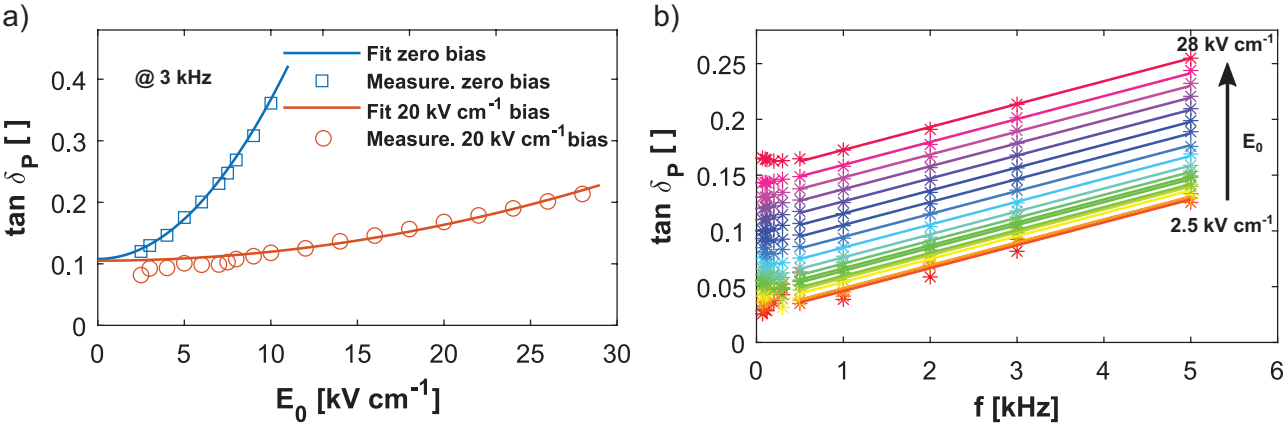

Figure 8. The polarization loss tangent as a function of a) field amplitude at 3 kHz and b) frequency for varying field amplitudes.

the field amplitude, but independent of frequency, and a constant loss term are found which can not be explained by the polarization rotation model in its present form. We speculate that the amplitude dependent loss term is related to the oscillation of the amount of bound charges in charged domain walls due to the angular oscillation of the polarization vectors in the domains at both sides of the domain wall. This would show up in the dielectric properties of the film and, thus, in the polarization hysteresis but not in the mechanical, hence, strain properties. This would explain why for the strain loss tangent no field amplitude dependence is observed. For the constant loss term $\tan\delta_0$ we speculate that it could be a material dependent term, which describes the energy needed to initialize the polarization rotation. As such, the decrease of this value for the bias case is reasonable as the bias field has already moved the polarization vector out of its equilibrium position and further movement is easier. As the measurement noise for the strain response is much higher than for the polarization response we are not sensible to the existence of such a term in the strain case. It is finally remarked that it is the extensive data set resulting from our study into the frequency and field amplitude dependence of the loss tangent that allows us to distinguish possibly different loss mechanisms in the same film. It also shows that several loss mechanisms with similar strength can be involved simultaneously. These results may be useful for further analysis with existing or new models for polarization loss.

4. Conclusions

In summary, we observe hysteretic strain behavior for an applied AC field superimposed on a DC bias field with a linear AC field amplitude response of the strain and a nonlinear, hysteretic polarization response in an epitaxial $PbZr_{0.55}Ti_{0.45}O_3$ film with a monoclinic symmetry. The strain and polarization amplitude responses are well explained by an extension of the polarization rotation model, by taking into account the effect of a DC bias field on the rotation of the polarization vector. The polarization rotation model with applied bias, can predict the reduction of the nonlinearity of the polarization amplitude response for the case of non-zero field bias as compared to the zero bias case. The strain loss tangent is fully accounted for by the viscous term in the strain model. Of interest is the observed additional field dependent term in the polarization loss tangent, which is attributed to a lossy charge motion mechanism in the ferroelectric film.

5. Experimental Section

The film used in the experiment was a 3 µm thick monoclinic $PbZr_{0.55}Ti_{0.45}O_3$ film sandwiched between 100 nm thick $LaNiO_3$ electrodes on a (001)-oriented single terminated $SrTiO_3$ substrate. For details on the film growth and crystallographic characterization see Lucke et. al.[26] The strain and polarization were measured with a double beam laser interferometer (aixDBLI) combined with the aixACCT TF-2000 Analyzer. For the hysteresis measurements an oscillatory field with variable frequency in the range $f = 70$ Hz to 5 kHz and amplitude E_0 in the range 2.5–28 kV cm^{-1} was used on top of a DC bias field of 20 kV cm^{-1}. This bias field was chosen to be equal to the coercive field at 1 kHz measurement frequency. In the hysteresis experiments a maximum AC field amplitude of 28 kV cm^{-1} was chosen so that even for the largest AC field amplitude due to the bias field one stays away safely from the coercive field at –20 kV cm^{-1} on the decreasing branch of the polarization loop. Before each hysteresis measurement the film was poled with a DC field of 200 kV cm^{-1} to realize comparable starting conditions. The phase angle accuracy of the aixACCT TF-2000 Analyzer was verified using a linear electrical component, that is a 1 MΩ resistor as explained in Section S6, Supporting Information.

Supporting Information

Supporting Information is available from the Wiley Online Library or from the author.

Acknowledgements

This work was part of the research programme "Smart Multilayer Interactive Optics for Lithography at Extreme UV wavelengths (SMILE)" with contract number 10448, and was financially supported by the Nederlandse Organisatie voor Wetenschappelijk Onderzoek (NWO) and Carl Zeiss SMT. This research had been carried out in the Industrial Focus Group XUV Optics and the Inorganic Material Science Group at the MESA+ Institute for Nanotechnology of the University of Twente. The Industrial Focus Group XUV Optics received further support from the Province of Overijssel, ASML, and Malvern Panalytical. The authors would like to thank Dr. James Byers of the Industrial Focus Group XUV Optics for proofreading the manuscript.

Conflict of Interest

The authors declare no conflict of interest.

Data Availability Statement

The data that support the findings of this study are available from the corresponding author upon reasonable request.

Keywords

ferroelectrics, hysteresis, nonlinearity, piezoelectric, thin film

Received: February 3, 2021
Revised: April 28, 2021
Published online:

[1] R. Waser, *Ceramic. Materials for Electronics; Processing, Properties, and Applications*, Vol. *4*, 2nd ed., Wiley, New York **1991**, p. 311.
[2] N. Setter, D. Damjanovic, L. Eng, G. Fox, S. Gevorgian, S. Hong, A. Kingon, H. Kohlstedt, N. Y. Park, G. B. Stephenson, I. Stolitchnov, A. K. Taganstev, D. V. Taylor, T. Yamada, S. Streiffer, *J. Appl. Phys.* **2006**, *100*, 5.
[3] P. Muralt, *J. Am. Ceram. Soc.* **2008**, *91*, 5.
[4] P. Muralt, R. G. Polcawich, S. Trolier-McKinstry, *MRS Bull.* **2009**, *34*, 9.
[5] C.-B. Eom, S. Trolier-McKinstry, *MRS Bull.* **2012**, *37*, 11.
[6] M. Bayraktar, W. A. Wessels, C. J. Lee, F. A. van Goor, G. Koster, G. Rijnders, F. Bijkerk, *J. Phys. D: Appl. Phys.* **2012**, *45*, 49.

[7] M. Bayraktar, A. Chopra, G. Rijnders, K. Boller, F. Bijkerk, *Opt. Express* **2014**, *22*, 25.
[8] M. Nematollahi, P. Lucke, M. Bayraktar, A. Yakshin, G. Rijnders, F. Bijkerk, *Opt. Lett.* **2019**, *44*, 20.
[9] H. Yang, F. Yan, Y. Lin, T. Wang, *ACS Sustainable Chem. Eng.* **2017**, *5*, 11.
[10] J. O. Gentner, P. Gerthsen, N. A. Schmidt, R. E. Send, *J. Appl. Phys.* **1978**, *49*, 8.
[11] B. Laikhtman, *Phys. Solid State* **1973**, *15*, 62.
[12] V. Postnikov, V. Pavlov, S. Gridnev, S. Turkov, *Phys. Solid State* **1968**, *10*, 6.
[13] V. Postnikov, V. Pavlov, S. Gridnev, B. Darinskii, I. Glozman, *Bull. Russ. Acad. Sci.: Phys.* **1967**, *31*, 1888.
[14] G. Arlt, H. Dederichs, *Ferroelectrics* **1980**, *29*, 47.
[15] D. Damjanovic, M. Demartin, *J. Phys. D: Appl. Phys.* **1996**, *29*, 7.
[16] L. Rayleigh, *London Edinburgh Dublin Philos. Mag. J. Sci.* **1887**, *23*, 142.
[17] L. Néel, *Cah. Phys.* **1942**, *12*, 1.
[18] L. Néel, *Cah. Phys.* **1943**, *13*, 861.
[19] G. Bertotti, *Phys. Rev. Lett.* **1996**, *76*, 10.
[20] G. Bertotti, V. Basso, G. Durin, *J. Appl. Phys.* **1996**, *79*, 8.
[21] K. Vergeer, Ph.D. Thesis, Universiteit Twente **2017**.
[22] S. Trolier-McKinstry, N. Bassiri Gharb, D. Damjanovic, *Appl. Phys. Lett.* **2006**, *88*, 20.
[23] R. E. Eitel, T. R. Shrout, C. A. Randall, *J. Appl. Phys.* **2006**, *99*, 12.
[24] C. Lian, Z. A. Ali, H. Kwon, B. M. Wong, *J. Phys. Chem. Lett.* **2019**, *10*, 12.
[25] V. I. Yukalov, E. P. Yukalova, *Phys. Rev. Research* **2019**, *1*, 3.
[26] P. Lucke, M. Bayraktar, Y. A. Birkhölzer, M. Nematollahi, A. Yakshin, G. Rijnders, F. Bijkerk, E. P. Houwman, *Adv. Funct. Mater.* **2020**, *30*, 52.
[27] N. Bassiri-Gharb, I. Fujii, E. Hong, S. Trolier-Mckinstry, D. V. Taylor, D. Damjanovic, *J. Electroceram.* **2007**, *19*, 47.
[28] D. Damjanovic, M. Demartin, *J. Phys.: Condens. Matter* **1997**, *9*, 23.
[29] D. V. Taylor, D. Damjanovic, E. Colla, N. Setter, *Ferroelectrics* **1999**, *225*, 91.
[30] B. Negulescu, C. J. M. Daumont, J. Sakai, A. Ruyter, M. Bavencoffe, N. Alyabyeva, J. Wolfman, *Ferroelectrics* **2017**, *514*, 9.
[31] E. P. Houwman, K. Vergeer, G. Koster, G. Rijnders, *Functional Properties of Polydomain Ferroelectric Oxide Thin Films*, Ch. 2, Springer, Berlin **2017**, 29–53.
[32] E. Houwman, K. Vergeer, G. Koster, G. Rijnders, *arXiv:1901.10883*, **2019**.